ACS NANO
Cite This: ACS Nano 2019, 13, 14459−14467
www.acsnano.org

ARTICLE

Click Reaction for Reversible Encapsulation of Single Yeast Cells

Wei Geng,[†,∥] Nan Jiang,[§] Guang-Yan Qing,[†] Xiaolong Liu,[∥] Li Wang,[†,‡] Henk J. Busscher,[⊥] Ge Tian,[†] Taolei Sun,[†] Li-Ying Wang,[#] Yunuen Montelongo,[▽] Christoph Janiak,[○] Guo Zhang,[¶] Xiao-Yu Yang,*[,†,§,∥] and Bao-Lian Su*[,†,‡]

[†]State Key Laboratory of Advanced Technology for Materials Synthesis and Processing, Wuhan University of Technology, 122, Luoshi Road, Wuhan, 430070, China

[‡]Laboratory of Inorganic Materials Chemistry (CMI), University of Namur, 61, Rue de Bruxelles, B-5000 Namur, Belgium

[§]School of Engineering and Applied Sciences, Harvard University, Cambridge, Massachusetts 02138, United States

[∥]Southern Marine Science and Engineering Guangdong Laboratory (Zhuhai) & School of Chemical Engineering and Technology & School of Materials, Sun Yat-Sen University, Guangdong, 510275, China

[⊥]Department of Biomedical Engineering, University of Groningen and University Medical Center Groningen, Antonius Deusinglaan 1, 9713 AV Groningen, The Netherlands

[#]State Key Laboratory of Magnetic Resonance and Atomic and Molecular Physics, Wuhan Institute of Physics and Mathematics, Chinese Academy of Sciences, Wuhan, 430071, China

[▽]Centro de Investigaciones en Óptica, A.C., Loma del Bosque 115, Colonia Lomas del campestre, León, PC 37150, Mexico

[○]Institut für Anorganische Chemie und Strukturchemie, Heinrich-Heine-Universität Düsseldorf, 40204, Düsseldorf, Germany

[¶]Key Laboratory of Environmental Health, Ministry of Education, Department of Toxicology, School of Public Health, Tongji Medical College, Huazhong University of Science and Technology, Wuhan, 430030, China

Supporting Information

ABSTRACT: **Cell surface engineering is an emerging technology to encapsulate cells in order to enhance their functions. However, methods for reversible encapsulation of cells with abiotic functionalities are rare. Herein, we describe a phenylboronic acid based click reaction for encapsulation of single yeast cells using mesoporous silica nanoparticles (MSNs). This encapsulation does not impact natural growth of the cells and leads to a significant enhancement of cell survival in a variety of hostile environments. Owing to the glucose-responsiveness of the boronate ester bond between cell surface polysaccharides and $B(OH)_2$-grafted MSNs, encapsulation was reversible by addition or removal of glucose. This effort offers living cells effective protection under harsh conditions and enables reversible assembling−detaching of abiotic functions.**

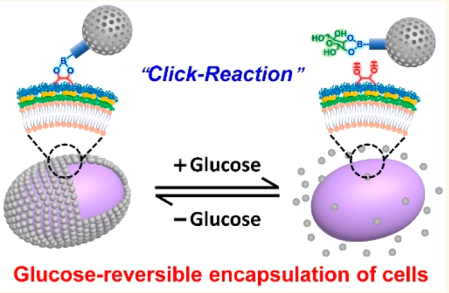

KEYWORDS: *click reaction, reversible encapsulation, cell stability, cell protection, directed chemistry, hierarchical assembly, mesoporous materials*

Cell surface engineering is an important, non-genetically-based technology[1−4] to encapsulate cells to endow them with abiotic functions and to enhance their viability under hostile conditions.[5−9] While many nanostructured materials[10−24] have been explored for use in single-cell encapsulation, most require encapsulation processes that are irreversible, and, as a result, the encapsulated cells have inhibited growth that results in the creation of an "artificial hibernating state".[25] Thus, a significant goal in the cell surface engineering area is to develop methods for encapsulation of cells within dynamic and degradable shells that leads to protection and regulation and which then can be removed to give cells possessing their native properties.[26−29] Although having numerous advantageous features, encapsulation protocols for reversible assembly and detachment of functionalities are not available.

In general, processes that take advantage of weak interactions possess high selectivity and tunability, and, as a result, they are used to fabricate dynamic nanostructures. However, the utilization of processes of this type for cell

Received: October 14, 2019
Accepted: December 5, 2019
Published: December 5, 2019

DOI: 10.1021/acsnano.9b08108
ACS Nano 2019, 13, 14459−14467

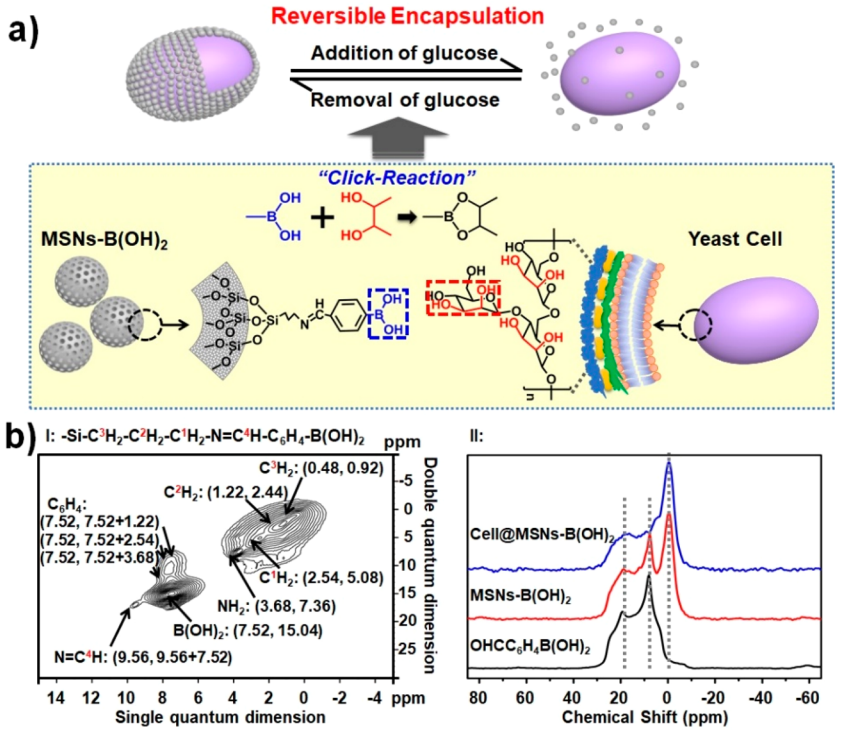

Figure 1. MSN-B(OH)$_2$ encapsulation of yeast cells through click reaction and characterization of the chemical composition of MSNs. (a) Schematic of reversible encapsulation of yeast cells with MSNs using a boronic acid vicinal-diol-based click reaction. Addition of glucose displaces MSN-B(OH)$_2$ from the cell surface polysaccharide, while removal of glucose by exposure to low pH leads to re-encapsulation by MSN-B(OH)$_2$. (b, I) ^{1}H DQ-SQ MAS NMR spectra of MSN-B(OH)$_2$ containing a Schiff-base-linked boronic acid group, and (b, II) ^{11}B CP/MAS NMR spectra of 4-formylphenylboronic acid and MSN-B(OH)$_2$ before and after cell encapsulation.

encapsulation encounters limitations associated with the stability of bonds formed between the nanomaterials and cell surfaces. Consequently, strong interactions between cell surfaces and added nanounits are required in order to generate stable nanofunctionalized cells. However, strong interactions, such as those arising through covalent bonding, often have drawbacks associated with the lack of reversible dynamics. In considering the design of encapsulation processes that would possess reversibility, we recognized that cis-diols containing polysaccharides are common and important components of cell surfaces. For example, the walls of yeast cells are mostly composed of cell surface polysaccharides (β-(1→3)-glucan, β-(1→6)-glucan, chitin, or mannoproteins[30]). Furthermore, it has been demonstrated recently that phenylboronic acid-based click reactions can be used to create covalent linkages to cis-diols of alcohols. We envisaged that a click reaction approach of this type could be applicable to bonding suitably modified nanounits to abundant cis-diol-containing polysaccharides on cell surfaces.[31,32] Moreover, click reactions between a boronic acid and cis-diols should be both rapid (often in seconds) and mild (neutral pH, aqueous solvent, room temperature, and mild pressure), and consequently they would not perturb cell surface proteins and cellular physiological processes. Of equal importance is the expectation that addition of high concentrations of glucose could be utilized to reverse this type of click reaction through competitive bonding to the phenylboronic acid.

In an investigation designed to evaluate the applicability of the phenylboronic acid-based click process, we realized that effective shells created in the encapsulation process need to have a degree of porosity that allows exchange of nutrients and waste while at the same time offering protection to the cells. Thus, mesoporous silica nanoparticles (MSNs) were selected as the model shell material because they are representative of typical high surface area, uniform open-framework nanocarriers, and biocompatible nanomaterials. In addition, yeast *Saccharomyces cerevisiae* cells were used in this exploratory investigation because of their common use as a model in shellization studies.[4] The current study has led to the development of a method for reversibly encapsulating single cells by a chemical process that directly bonds cell-surface polysaccharides to phenylboronic acid-linked MSNs. The effort has also demonstrated that shells created in this manner not only protect the cells in harsh environments, but also can be readily removed and self-assembled by simply controlling the concentration of glucose in the media.

RESULTS AND DISCUSSION

Modification of MSNs. Figure 1a presents the click reaction chemistry applied to reversibly encapsulate a yeast cell with a nanoporous shell. The B(OH)$_2$-containing mesoporous silica nanoparticles (MSN-B(OH)$_2$) employed in the click reaction with yeast cells were prepared by the Schiff-base-forming reaction of 4-formyphenylboronic acid with 3-aminotriethoxysilane (APTES)-modified MSNs (see Note S1). The observation of correlated double quantum dimensions at (9.56, 9.56 + 7.52) (Figure 1b I) demonstrates that the N═CH proton in MSN-B(OH)$_2$ resides in close proximity to the benzene ring.[33] Additional support for this conclusion comes from the observation of four resonances at 61.5, 128.5, 134.0, and 164.0 ppm in the ^{1}H−^{13}C CP/MAS NMR spectra (Figure S2a and d) and confirmed by IR spectra showing the disappearance of the −CHO (aldehyde)

DOI: 10.1021/acsnano.9b08108
ACS Nano 2019, 13, 14459−14467

absorption band at 2750 cm^{-1} (Figure S3a, spectra III and IV). Both indicate successful grafting-on of $B(OH)_2$. Note that not all silicon hydroxyl groups on the surface are involved in grafting-on of MSN-$B(OH)_2$ (see Figure S2f), which enable self-packing of nanoparticles around the cell surface.

Encapsulation of Yeast Cells by Using MSN-$B(OH)_2$. Encapsulation was carried out by gently shaking a suspension of a mixture of MSN-$B(OH)_2$ and yeast cells in phosphate-buffered saline (PBS; pH 7.0) at room temperature for 5 min. Evidence for rapid grafting of MSNs to the hydroxyl groups of polysaccharides on the cell surfaces comes from the observation of changes in ^{11}B NMR spectra in the 7.0−8.0 ppm region (Figure 1b II). The obvious changes of line shape and signal intensity from 4-formyphenylboronic acid reflect the fact that the boron hydroxyl groups grafted-on MSNs have become bonded with hydroxyl groups of polysaccharides on the yeast cell surface. Assembly of MSN-$B(OH)_2$ on the surface does not affect the cell shape (compare Figure 2a−d and Figure S4). However, the MSNs-$B(OH)_2$ layer on the cell is disordered (Figure 2a, inset), a likely result of elastic stresses known to be induced by the Gaussian curvature of the cell surface[34] and localized effects of high charged protein sites.[35] Scanning transmission electron microscopy (STEM) and TEM images of the encapsulated cells (Figure 2b inset, c, and d) show that the MSN-$B(OH)_2$ shells surrounding the cells have thicknesses of about 100−150 nm, suggesting the existence of only three to four layers of the MSNs. This conclusion, which is also consistent with the diameter of the MSNs prior to and after grafting-on of boron hydroxyl groups (compare Figure 2c, inset, and Figure S5), suggests that MSN-$B(OH)_2$ intimately couples to the native cell surface. Individual MSN-$B(OH)_2$, observed by inspecting the TEM micrograph shown in the inset in Figure 2c, have a diameter of about 40 nm, which corresponds to the value derived by using dynamic light scattering (DLS; Figure S6a and c−e). Note that MSN-$B(OH)_2$ has a slightly smaller pore diameter (2.2 nm) than do pure MSNs (2.7 nm; Figure S7), and in contrast to the MSNs they self-aggregate as a consequence of hydrogen bonding and attractive Lifshitz−van der Waals forces of the residual OH[36] to form aggregates with a roughly 4-fold larger diameter and a wider diameter distribution (compare Figure S6c and e). Voids and secondary porosity, which unavoidably form during nanoparticle encapsulation of cells,[37] along with the inherent porosity of MSN-$B(OH)_2$, which have a BET surface area of 197 m^2/g (Figure S7 and Table S1), combine to create nanoporous MSN-$B(OH)_2$ shells encapsulating the cells. The encapsulated cells display an energy-dispersive X-ray spectroscopy (EDX) line scan that shows a higher Si content at the position of the cells (Figure 2e) and an EDX area scan that shows a uniform distribution of Si on the cell surface (Figure 2f).

Viability and Protection against Hostile Environments of Yeast after Encapsulation. Encapsulation by MSN-$B(OH)_2$ does not negatively affect the viability of yeast cells (Figure 3 and Figure S9). Moreover, cells encapsulated by MSN-$B(OH)_2$ show a higher viability following a 6 d exposure to water, a time period over which near complete death of native cells takes place (Figure 3). Furthermore, MSN encapsulation bestows protection to the cells against a number of hostile conditions ($p < 0.01$; Student's t test, see Table S2), including elevated temperature, UV light, lyticase, and osmotic shock, with respective percent survivals of 71 ± 3%, 95 ± 1%, 84 ± 2%, and 96 ± 1% remaining, in contrast to percent survivals of native cells of 27 ± 2%, 17 ± 5%, 41 ± 8%, and 21 ± 3%.

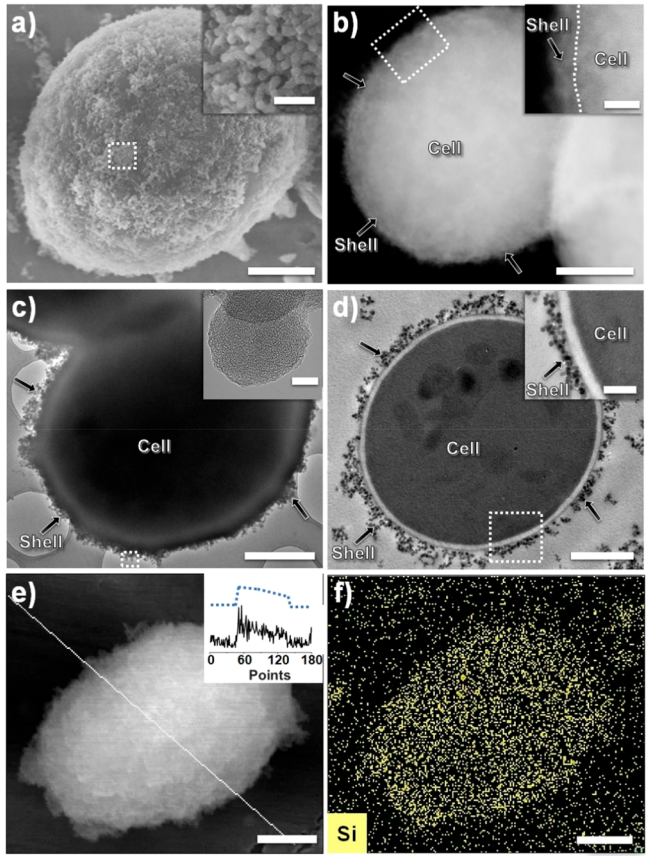

Figure 2. Surface characteristics of single MSN-$B(OH)_2$-encapsulated yeast cells. (a) SEM micrograph of an encapsulated cell at low magnification (scale bar 1 μm) and SEM micrograph of MSN-$B(OH)_2$ in the porous shell (inset) at high magnification (scale bar equals 200 nm). (b) STEM micrograph of a MSN-$B(OH)_2$-encapsulated cell at low magnification (scale bar 1 μm) and the inset at high magnification (scale bar 200 nm). (c) TEM micrograph of an encapsulated cell at low magnification (scale bar 1 μm) and TEM micrograph of the mesoporous structure of an MSN-$B(OH)_2$ shell around an encapsulated yeast cell (scale bar equals 10 nm). (d) TEM micrograph of a microtome-sliced encapsulated cell at low magnification (scale bar equals 1 μm) and the inset at high magnification (scale bar 300 nm). (e) EDX Si-line scan of an MSN-$B(OH)_2$-encapsulated cell and (f) Si-map of the encapsulated cell taken along the white line shown in the SEM micrograph (scale bar 1 μm).

To evaluate MSN-$B(OH)_2$-encapsulated cells created by using the boronate-diol click process, polyelectrolyte-assisted silica-encapsulated (NSN-PDDA) cells, formed by using nonporous silica nanoparticles and poly(diallyldimethylammonium chloride), were used for comparison purposes. Observations show that both NSN-PDDA- and MSN-$B(OH)_2$-encapsulated yeast cells display higher protection against heat uptake as compared to that of native cells. In addition, cells that contain an MSN-$B(OH)_2$ shell in liquid suspension (Figure S10a) maintain a lower temperature upon heating than do NSN-PDDA-encapsulated cells. Eventually the encapsulated cells will be in a thermodynamic equilibrium with their environment regardless of shellization and adapt to the environmental temperature (Figure S10b and c). Also, click-reaction-formed MSN-$B(OH)_2$-encapsulated cells exhibit

DOI: 10.1021/acsnano.9b08108
ACS Nano 2019, 13, 14459−14467

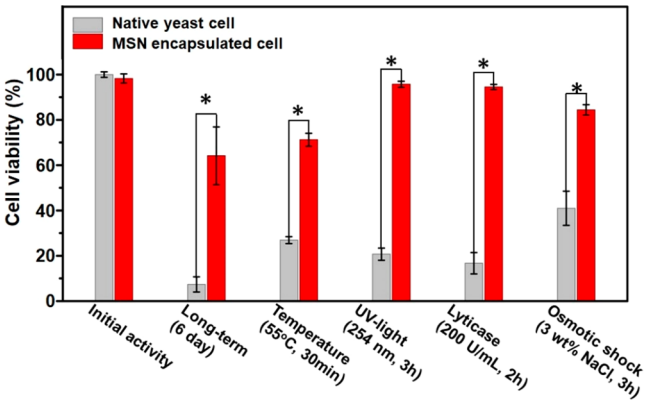

Figure 3. Protection against different hostile environmental conditions caused by MSN-B(OH)$_2$ encapsulation of native yeast cells. To assess the protection ability engendered by MSN-B(OH)$_2$ encapsulation, the yeast cells were stained with FDA/PI and then evaluated using microscopy. Data used to calculate percent viabilities in the cultures, with error bars indicating standard deviations over 1000−1500 cells, come from five separate experiments with different batches of yeast cultures. The * indicates significant differences at $p < 0.01$ (Student's t test) between native and MSN-encapsulated yeasts.

much higher UV absorption than do NSN-PDDA cells (Figure S11) because of the presence in the former of the benzaldimine chromophore. The largest difference in protection offered by MSN-B(OH)$_2$ versus NSN-PDDA encapsulation was observed in lyticase exposure experiments. Although both MSN-B(OH)$_2$ and NSN-PDDA have the ability to adsorb lyticase (Figure S12), cells encapsulated with NSNs do not survive exposure to lyticase. The finding that NSN-encapsulated yeast cells have only 16% viability after exposure to lyticase (Figure 3) suggests that leakage of lyticase through the NSN shell in combination with the known cell wall damaging effect of cationic polyelectrolytes[38] such as PDDA leads to death of NSN-PDDA-encapsulated cells. Finally, click-reaction-promoted MSN-B(OH)$_2$ encapsulation provides a protection effect against osmotic shock similar to NSN-PDDA encapsulation. This finding indicates that the structural rigidity of both shells is strong enough to enable cells to withstand osmotic pressure changes.

MSN-B(OH)$_2$ encapsulation does not affect the growth of yeast cells (Figure S13), likely because of fast and efficient nutrient diffusion through the encapsulating shell. This phenomenon is different from polyelectrolyte-assisted nonporous silica nanoparticle (NSNs, colloidal silica) encapsulation, which causes a lag time of *ca.* 5−6 h before cell growth begins. Also, the results of independent membrane diffusion experiments (Figure S14a), using membrane filters on which MSN-B(OH)$_2$ and NSN-PDDA layers are applied, demonstrate that glucose more rapidly diffuses through MSN-B(OH)$_2$ layers than NSN-PDDA layers (Figure S14b and c). A slightly higher level of glucose adsorption occurs by using the MSN-B(OH)$_2$ layer as compared with its NSN-polyelectrolyte (Figure S14d and e), reflecting a higher glucose storage capacity of click-reaction-formed MSN-B(OH)$_2$ shells.

Immediately after mixing with MSN-B(OH)$_2$, yeast cells become encapsulated within nanoporous layers of MSN-B(OH)$_2$. As time proceeds, daughter cells arise that are less evenly covered with MSN-B(OH)$_2$ shells (Figure S15). Thus, the MSN-B(OH)$_2$ shells allow continued growth of the cells, thus preventing them from entering an undesirable hibernating state.[25] MSN-B(OH)$_2$ coverage decreases with production of each generation of cells, as can be seen by comparing micrograph images taken 1.5, 3.0, and 4.5 h after beginning the encapsulation process. Owing to the strong covalent interactions between MSN-B(OH)$_2$ and polysaccharides on their surfaces, the mother cells remain traceable in the micrographs. Meanwhile, the concentration of glucose continuously decreases during 1 day of culture, while Si element in solution remains relatively balanced with slight change (Figure S16), which also means that MSNs are stably binding with mother cells. It should be noted that the degrees of protection offered by encapsulation using all types of cell surface engineering methods decrease with formation of ensuing generations of daughter cells. This is an important feature that distinguishes cell surface engineering from genetic engineering and that enables avoidance when needed of the risk of creating organisms with permanent properties such as resistance to antimicrobial agents.

Reversibility of MSN-B(OH)$_2$ Encapsulation. It is necessary to point out that the decrease of stability and loss of nanofunctional features of encapsulated cells and/or daughter cells often occur as a result of damage to shell structures caused by cell division. This issue can be addressed by developing reversible encapsulation processes, the direction of which can be governed by simple manipulations. The glucose and pH responsiveness of phenylboronic acid ester formation and cleavage[32] provides a method to detach MSN-B(OH)$_2$ shells that serves as an alternative to using on-demand degradable shells to prevent undesirable permanent shell coverage and cell hibernation.[25−29] Moreover, our developed method also enables reorganization of single-cell encapsulation by shell reassembly. As illustrated in Figure 4a, MSN-B(OH)$_2$ detachment from the surface of a yeast cell should occur upon addition of glucose at pH 7 by driving the click reaction equilibrium toward glucose binding with phenylboronic acid, which disrupts the borate-ester linkage between MSN-B(OH)$_2$ and cis-diol groups in the cell surface polysaccharides. Furthermore, upon removal of glucose by decreasing the pH to 6.0, the phenylboronic acid ester linkage between MSN-B(OH)$_2$ and cell surface polysaccharides should re-form at pH 7.0 (see Figure 1a). The reversibility of the click process, like the properties of biodegradable shells,[26−29] enables on demand removal of the MSN-B(OH)$_2$ shell, and it also provides a pathway for enabling MSN-B(OH)$_2$ encapsulation of daughter cells during cell growth (Figure 4b, left). Because MSN-B(OH)$_2$ encapsulation can be carried out without the need for chemical modification of the cell surface, the generated daughter cells can be easily re-encapsulated by simply adding MSN-B(OH)$_2$ grafted to the cell culture medium (see right part of Figure 4b).

In order to investigate more fully the reversibility of click-reaction-induced MSN-B(OH)$_2$ encapsulation, binding of mannose and glucose to B(OH)$_2$ gold-coated crystal surfaces was evaluated using a quartz crystal microbalance (QCM). Both glucose and yeast-extract-peptone-dextrose (YPD) have a much higher affinity for B(OH)$_2$ groups than does mannose and are completely reversed at pH 6 unlike that of mannose (Figure 4c). The amount of glucose that becomes bound to B(OH)$_2$ groups following initial addition of mannose is higher than the original amount of bound mannose, and binding of both monosaccharides is fully reversed upon exposure to pH 6.0 buffer (Figure 4d). Since glucose binding is fully reversible

DOI: 10.1021/acsnano.9b08108
ACS Nano 2019, 13, 14459−14467

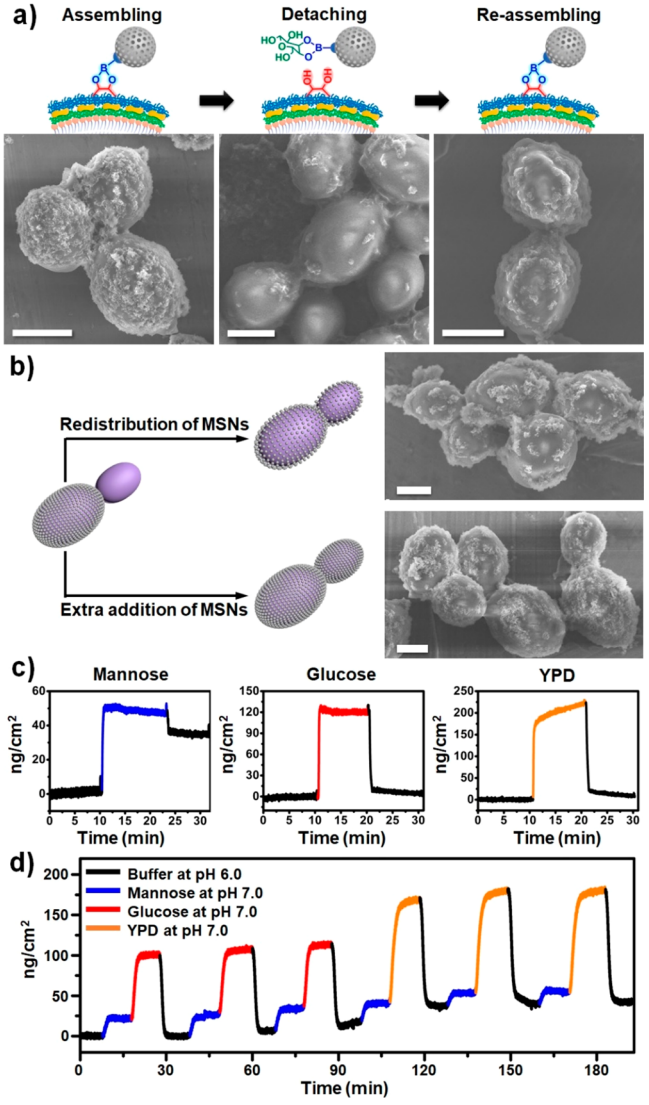

Figure 4. Reversible MSN-B(OH)$_2$ encapsulation of *S. cerevisiae* cells. (a) SEM micrographs of MSN-B(OH)$_2$-encapsulated cells (1) before and (2) after MSN-B(OH)$_2$ dissociation promoted by addition of glucose (20 mg/mL) at pH 7.0, and (3) following reassembly caused by glucose removal at pH 6.0. (scale bar 3 μm). (b) Micrographs of cells (right-upper panel) following glucose addition and dilution, which causes redistribution of MSN-B(OH)$_2$ over daughter cells and (right-lower panel) of cells following addition of extra MSN-B(OH)$_2$, which leads to complete restoration of encapsulation of daughter cells (scale bars 2 μm). (c) Quartz crystal microbalance determinations of the amounts of binding of mannose (18 μg/mL), glucose (20 mg/mL), and yeast-extract-peptone-dextrose components containing 20 mg/mL glucose to B(OH)$_2$ gold-coated crystal surfaces before and after exposure to pH 6.0 buffer. (d) Quartz crystal microbalance determinations of the amounts of binding to B(OH)$_2$ gold-coated crystal surfaces following consecutive addition of mannose and either glucose or YPD before and after exposure to pH 6.0 buffer.

while mannose binding is only partially reversible at pH 6 (Figure 4c), it appears that added glucose displaces mannose from the B(OH)$_2$ groups. Consecutive binding of YPD components, which contain not only glucose but also peptone and yeast extract, including polypeptides, amino acids, and nucleotides, displays a pattern that is similar to consecutive glucose binding, with the exception that it is less reversible (see also Figure 4d). This finding is likely a consequence of the inability of the YPD complex to displace mannose from the B(OH)$_2$ groups. Note that *S. cerevisiae* is able to fully survive high glucose concentrations up to at least 20 mg/mL (Figure S17).

CONCLUSIONS

In summary, MSNs were directly, stably, and reversibly coupled by using B(OH)$_2$ click reaction chemistry of the polysaccharides abundantly present on yeast cell surfaces to form a nanoporous shell while maintaining viability. Click-reacted MSN-B(OH)$_2$ shells showed superior growth and significant protection against different hostile environmental conditions. The features and advantages of click-reacted MSN protection have been thoroughly investigated. Importantly, the reversibility gives the encapsulation process the ability to detach and reassemble shells over several daughter cell generations and to add nanoparticle functionalities without the need for chemical modification. Consequently, the click-based method should be highly versatile for introducing protective capsules and controllable assembly disassembly nanofunctionality around single cells as part of biotechnological efforts.

MATERIALS AND METHODS

Chemicals. Tetraethylorthosilicate (TEOS), 3-aminopropyltriethoxysilane (APTES), diethanolamine (DEA), cetyltrimethylammonium chloride solution (CTAC), 4-mercaptophenylboronic acid, pyrogallol, 4-formylphenylboronic acid, and polyamide powder were purchased from Aladdin Industrial, China. Peptone, TE buffer solution (pH 8.0), and yeast extract were purchased from Sangon Biotech (Shanghai) Co., Ltd., China. Ethanol, toluene, D-(+)-mannose, D-(+)-glucose, ammonia solution (25−28%), NaCl, hydrochloric acid (36−38%), KH_2PO_4, $Na_2HPO_4{\cdot}2H_2O$, formic acid, and acetic acid glacial were purchased from Sinopharm Chemical Regent Co., Ltd., China. Poly(diallyldimethylammonium chloride) solution (20 wt % in water, PDDA), glucose oxidase (GOX), peroxidase (HRP), and poly(sodium 4-styrenesulfonate) (MW ≈ 70 000, PSS) were purchased from Sigma-Aldrich Co. (USA). Lyticase was purchased from Shanghai Yuanye Bio-Technology Co., Ltd. Unless otherwise noted, all reagent-grade chemicals were used as received.

Cell Culturing and Harvesting. *Saccharomyces cerevisiae* was purchased from the China Center of Industrial Culture Collections and stored as a frozen stock, kept at −70 °C. Yeast from the frozen stock were grown overnight at 30 °C on a YPD agar stock plate that was never kept longer than one month. For culturing, a single colony of yeast cells was picked from the agar stock plate and grown in YPD broth (4 g yeast extract, 8 g glucose, and 4 g peptone in 400 mL H_2O) in a shaking incubator at 30 °C for 24 h to an optical density OD_{600} of around 1.0. Yeast were harvested by centrifugation of a 4 mL culture at 3500 rpm for 5 min and washed twice with PBS at pH 7.0 (0.4 mol/L KH_2PO_4, 0.6 mol/L $Na_2HPO_4{\cdot}2H_2O$) to remove excessive medium, and the pellet obtained after centrifugation was immediately used for further studies.

Mesoporous Silica Nanoparticles. MSNs were synthesized as described before.[39] Briefly, 10.4 g of CTAC (25 wt % in water) and 0.2 g of DEA were first dissolved in a solution of 64 mL of deionized water supplemented with 9.0 g of ethanol under stirring in an oil bath at 60 °C. After stirring for 30 min, 7.3 mL of TEOS was added, also under stirring (3 h at 60 °C) to yield a white, colloidal suspension. Next, nanoparticles were centrifuged and washed with an excess amount of water and ethanol and finally dried under vacuum. After drying, synthesized MSNs were refluxed in 120 mL of ethanol supplemented with 30 mL of hydrochloric acid (36−38%) overnight to extract all surfactants, yielding a white powder that was subsequently dried under vacuum.

DOI: 10.1021/acsnano.9b08108
ACS Nano 2019, 13, 14459−14467

Amino-Modified Mesoporous Silica Nanoparticles (MSNs-NH_2). A 0.2 g amount of MSN powder was suspended in anhydrous toluene (100 mL), after which 0.15 mL of APTES was added. The suspension was refluxed overnight at 70 °C, centrifuged, and washed with an excess amount of ethanol, and the powder obtained was dried under vacuum.

Boron Hydroxyl-Modified Mesoporous Silica Nanoparticles (MSNs-$B(OH)_2$). A 0.1 g amount of the MSNs-NH_2 powder and 0.1 g of 4-formylphenylboronic acid were mixed in anhydrous toluene (100 mL), and a few drops of acetic acid glacial were added. The suspension was refluxed at 70 °C overnight, after which particles were harvested, as described above for MSNs-NH_2. MSNs-$B(OH)_2$ were suspended in 30 mL of PBS (pH 7.0) at a concentration of 2 mg/mL.

Nonporous Silica Nanoparticles. NSNs were synthesized using the Stöber method.[40] Briefly, 15 mL of ammonia solution (25−28%) was added to a 250 mL ethanol solution. After the mixture was stirred at room temperature for 30 min, 15 mL of TEOS was dissolved in the solution, also under stirring (8 h at room temperature), to yield a white colloidal suspension. Next, nanoparticles were centrifuged and washed with an excess amount of water and ethanol and finally dried under vacuum, yielding a white powder.

Encapsulation of Yeast Cells. Yeast were encapsulated with silica nanoparticles according to our boron hydroxide click-reaction proposed and according to an interfacial-assisted encapsulation method for control. For boron hydroxyl-based click reaction between MSNs-$B(OH)_2$ and cell surface polysaccharides, the yeast pellet obtained after centrifugation of a 4 mL culture was mixed with 1 mL of a MSNs-$B(OH)_2$ suspension in PBS at room temperature for 5 min, after which encapsulated yeasts were collected by centrifugation and washed twice in PBS (3500 rpm, 5 min) as described above and resuspended in 1 mL of PBS. For control, interfacial-assisted layer encapsulation of yeast cells was done.[41] Briefly, the yeast pellet was added to a 1 mL PDDA solution (2.5 mg/mL) and shaken for 5 min to disperse the pellet, after which the resulting suspension was centrifuged again and the pellet obtained was mixed with a 1 mL suspension of NSNs in PBS (0.1 wt %) at room temperature for 5 min. NSN-encapsulated yeasts were subsequently obtained as described above for MSN-encapsulated yeasts. Native yeast suspensions were obtained by dispersing the initial pellet, obtained after culturing and centrifugation, in PBS.

Solid-State NMR Measurements. Solid-state $^{1}H-^{13}C$ cross-polarization magic angle spinning (CP/MAS) and ^{29}Si and ^{11}B high-power decoupling NMR experiments were performed on a Bruker AVANCE-III 500 spectrometer using a 4.0 mm MAS probe with a spinning rate of 12.5 kHz, a ^{1}H $\pi/2$ pulse length of 3.85 μs, a TPPM ^{1}H decoupling of 65 kHz, and a recycle delay of 5 s. ^{1}H MAS and 2D ^{1}H DQ-SQ MAS NMR spectra were carried out in a 1.9 mm MAS probe on a Bruker AVANCE-III 500 spectrometer with a sample spinning rate of 40 kHz, a ^{1}H $\pi/2$ pulse length of 1.75 μs, and a recycle delay of 2 s. The chemical shifts of ^{1}H, ^{13}C, and ^{29}Si were referenced to tetramethylsilane.

IR Spectroscopy. Fourier transform infrared (FTIR) spectroscopy was performed on a Bruker Vertex 80 V FTIR spectrometer, equipped with a single-reflection ATR ZnSe crystal.[42] Nanoparticle powders after various stages of modification were pressed into sample stage holes, after which spectra were recorded between 4000 and 400 cm^{-1} at a spectral resolution of 4 cm^{-1} and a data point resolution of 1 point per wavenumber. The digitized spectra were stored on an auxiliary computer and analyzed with OPUS/IR FTIR software (Bruker).

Zeta Potential Measurements and Dynamic Light Scattering. Electrophoretic mobilities were measured with a Zeta Sizer Nano Series (ZEN 3600, Malvern) using automatic voltage selection. A 1 mg amount of NSNs, MSNs, MSNs-NH_2, or MSN-$B(OH)_2$ powder was suspended in 20 mL of PBS (pH 7.0), and measurements were taken at 25 °C, after which electrophoretic mobilities were converted to zeta potentials using the Smoluchowski equation.[43] Hydrodynamic diameters of the mesoporous and nonporous nanoparticles used were measured with the same instrument.

Electron Microscopy on Mesoporous Silica Nanoparticles. SEM (S-4800, Hitachi, Japan) was used at 5 kV to observe the morphology of the nanoparticles. To this end, the powder pellet after centrifugation was dispersed in distilled water and a suspension droplet placed on the specimen stage of the microscope and dried for 30 min at 60 °C.

Porosity of Mesoporous Silica Nanoparticles through N_2 Adsorption−Desorption Isotherms. The N_2 adsorption−desorption isotherms were measured by a Micromeritics ASAP 3020 system. Nanoparticle powders were put in tubes and kept under vacuum for 6 h at 120 °C for degassing, after which the powder was weighed and the tube was fixed in the instrument and connected to a nitrogen cylinder for automated pressure increase/decrease, while keeping the tube in liquid nitrogen. Particle surface areas and pore size distributions were subsequently calculated from the adsorption isotherms according to Brunauer−Emmett−Teller and Barrett−Joyner−Halenda, respectively.[44]

Electron Microscopy on Encapsulated Yeast Cells. SEM and EDX were conducted on an S-4800 (Hitachi, Japan) to observe the morphology of the yeasts and visualize the distribution of silica (nanoparticles) over a cell surface, respectively. To this end, the yeast pellet was treated as described above and dried for 10 min at 40 °C in ambient air. The SEM was operated at 5 kV, while EDX was used at 30 kV with a distance between the electron gun and the sample of about 15 mm and Amp time set at 51.2 μs. In order to obtain ultrathin sections of encapsulated yeast cells suitable for transmission electron microscopy, pelleted yeasts were fixed overnight in 0.5% glutaraldehyde and postfixed for 1 h with 1% osmium tetroxide. After dehydration through an acetone−ethanol series, the sample was embedded in Epon 812/Araldite M resin. Thin sections with a thickness of around 100 nm were cut by using an ULTRACUT UCT ultramicrotome (Leica, Germany), and TEM micrographs were taken on a Tecnai microscope (The Netherlands), operated at 200 kV.

Growth Kinetics of Native and Encapsulated Yeast Cells. Growth kinetics of native and encapsulated yeast cells were determined for yeasts suspended in 50 mL of fresh YPD broth, and optical densities were measured every 2 h up to 24 h at 600 nm using a UV−vis spectrometer (UV-2550, Shimadzu, Japan) at a regular growth temperature of 30 °C.

Cell Viability Assay. Cell viability was investigated immediately after encapsulation by fluorescein diacetate/propidium iodide (FDA/PI) staining of the yeast.[45] FDA is hydrolyzed to green-fluorescent fluorescein by esterases in metabolically active cells, while PI is a red fluorescence dye that binds to DNA in necrotic or apoptotic cells. The FDA stock solution (5 mg/mL) was prepared in acetone, while the PI stock solution (1 mg/mL) was prepared in PBS (pH 7.0). A 10 μL amount of the FDA stock solution and 10 μL of the PI stock solution were mixed with 1 mL of PBS (pH 7.0) containing the yeast suspension, the mixture was incubated for 30 min at 30 °C, and cells were washed with PBS (pH 7.0). Routinely, five fluorescence images, containing between 200 and 300 cells, were taken on an inverted fluorescence microscope (Olympus IX53, Japan), and the ratio between the number of green and red fluorescent cells was taken as a measure of viability.

Diffusion and Absorption Experiments of Glucose through Click-Reacted MSN-$B(OH)_2$ and NSN-PDDA Layers. Glucose diffusion was studied through nanoparticle layers on 0.2 μm pore-size polycarbonate membrane filters (diameter 5 cm; JinTeng, Tianjin, China). Filter membranes were used as received or after depositing a nanoparticles layer with a similar thickness of MSNs-$B(OH)_2$ or NSNs-PDDA as in cell encapsulation. After deposition, membranes were air-dried at 60 °C under vacuum. For diffusion experiments, membranes with or without nanoparticle layers were fixed between two compartments, filled with 100 mL of water or 100 mL of glucose solution (20 mg/mL). Solution aliquots (1 mL) were taken every 10 min from the water-filled compartment, and glucose concentrations were measured. Glucose concentration was measured using a GOX and HRP coupled enzyme activity assay. Briefly, 10 μL of GOX (2 mg/mL), 10 μL of HRP (2 mg/mL), 250 μL of pyrogallol (50 mg/mL), 250 μL of glucose solution, and 2.5 mL of water were mixed in a

DOI: 10.1021/acsnano.9b08108
ACS Nano 2019, 13, 14459−14467

UV−vis cuvette and incubated for 30 min at 37 °C under shaking, and fluorescence emission was measured at 420 nm. Fluorescence was expressed as absolute amounts of glucose using a calibration curve. Absorption experiments were carried out similarly to that described above for diffusion, but only involved the compartment filled with a glucose solution and with the nanoparticle layer deposited on a nonporous surface to prevent diffusion through the layer.

Reversibility of Boron Hydroxyl-Based Click-Reaction-Based Shell. Primary MSN-$B(OH)_2$-encapsulated yeasts were suspended in 2 mL of glucose (20 mg/mL) in PBS (pH 7.0) and gently mixed at room temperature for 30 min to detach the MSN shell. Next cells were collected by centrifugation at 3500 rpm for 5 min, and the supernatant was centrifuged at 8000 rpm for 15 min to collect the MSNs. Subsequently cells were either processed for SEM as described above or kept for secondary encapsulation. For secondary encapsulation, nanoparticles with glucose bound to the $B(OH)_2$ were first suspended in PBS with pH adjusted to pH 6.0 by addition of KH_2PO_4 to remove glucose from the MSNs under gentle mixing at room temperature for 30 min. Next cells and MSNs were suspended again in PBS at pH 7.0 for the formation of a secondary shell. Since the high concentration of glucose applied might influence the viability of the yeast, the viability of the yeast after exposure to high glucose concentrations was determined. To this end, yeast suspensions were supplemented with different concentrations of glucose ranging from 0 to 20 mg/mL in in a shaking incubator at 30 °C for 1 h, after which cell viability was assessed using the FDA/PI assay.

Quartz Crystal Microbalance Measurements. The relative affinities of mannose, glucose, and YPD components for $B(OH)_2$ were determined using a QCM (Q-Sense E1 system, Sweden) at 25 °C using a Q-Sense E1 system (Sweden). A gold-coated quartz sensor was immersed in a boiling solution of ethanol, water, and ammonia (1:1:1 in volume) at 70 °C for 15 min and dried under nitrogen gas. Next the sensor was immersed in a 20 mL 4-mercaptophenylboronic acid solution in ethanol (1 mg/mL) to graft $B(OH)_2$ to the surface and dried under nitrogen gas. After insertion of the $B(OH)_2$ sensor in the QCM chamber, the chamber was perfused at a flow rate of 100 μL/min with deionized water followed by PBS at pH 7.0 until a stable frequency shift could be measured. Then, the chamber was perfused at a similar flow rate with either mannose (18 μg/mL), glucose (20 mg/mL), or YPD (containing besides peptone and yeast extract, 20 mg/mL glucose) until stable frequency shifts were observed, after which the chamber was perfused with PBS at pH 6.0 to observe possible desorption of mannose, glucose, or YPD components, respectively. The crystal was brought into resonance at 5 MHz, and the adsorbed mass to the crystal surface calculated employing the Sauerbrey equation:[7,46]

$$\Delta m = -\frac{C_{QCM}}{n}\Delta f \quad (1)$$

in which Δm is the amount of adsorbed mass, Δf is the shift in resonance frequency, CQCM is a mass sensitivity constant (17.7 ng/cm^2 for a 5 MHz crystal), and n is the overtone number of the resonance frequency used. All binding curves were recorded by Q-Sense software and analyzed by QTools using the third overtone (n = 3). Finally in a separate experiment, in order to study the effect of a high glucose concentration or YPD on mannose binding to a $B(OH)_2$-coated crystal surface, the QCM chamber was exposed to a flowing solution of mannose (18 μg/mL) for 10 min, followed by perfusion of the chamber with PBS at pH 7.0, after which glucose at a high concentration (20 mg/mL) or YPD was consecutively perfused through the system for another 10 min. The reversibility of the entire adsorption process was monitored by perfusing the chamber with PBS at pH 6.0.

Comparison of the Protection Offered by MSN-$B(OH)_2$ and NSN-PDDA Shells. Protection offered by MSNs-$B(OH)_2$ or NSNs-PDDA shells to *S. cerevisiae* was compared to native yeasts by exposing cells to five hostile environments. First, native and encapsulated yeast cells were exposed in pure water for 6 days, and their viability were evaluated by FDA/PI staining. Second, yeast cells were exposed for 30 min to an elevated temperature of 55 °C, and their viability was assessed using FDA/PI staining. Third, yeast suspensions in PBS (pH 7.0) were transferred to quartz tubes and exposed to UV light (254 nm) for 3 h. After irradiation, the cells were collected, and their viability was evaluated by the FDA/PI assay. Fourthly, cells were suspended in 1 mL of TE buffer (pH 8.0) supplemented with 20 μL of a lyticase solution (10 kU lyticase in 500 μL of glycerol and 500 μL of TE buffer (pH 8.0)) for 2 h at 37 °C under shaking, and their viability was evaluated. Finally, cells were subjected to an osmotic shock by suspending them for 3 h at 30 °C in PBS supplemented with 3 wt % NaCl at pH 7.0.

ASSOCIATED CONTENT

Supporting Information

The Supporting Information is available free of charge at https://pubs.acs.org/doi/10.1021/acsnano.9b08108.

Movie S1: Simulated heat transfer through MSN shell and NSN shell from the surroundings (MP4)

SEM, TEM, and fluorescence images, diameter distributions, NMR, FTIR, and UV−vis spectra, N_2 adsorption−desorption isotherm results, growth curves of cells, temperature images, diffusion and absorption of glucose, and zeta potentials; Note S1, detailed description of the MSNs-$B(OH)_2$ modification; Note S2, detailed description of MSNs-$B(OH)_2$ encapsulation *vs* NSN encapsulation; Note S3, detailed description of QCM data of YPD; Note S4, detailed description of ability of lyticase to diffuse in the shells (PDF)

AUTHOR INFORMATION

Corresponding Authors

*E-mail: xyyang@whut.edu.cn; xyyang@seas.harvard.edu.
*E-mail: baoliansu@whut.edu.cn; bao-lian.su@unamur.be.

ORCID

Nan Jiang: 0000-0001-8394-3247
Xiaolong Liu: 0000-0002-7346-7846
Taolei Sun: 0000-0002-3336-0788
Christoph Janiak: 0000-0002-6288-9605
Xiao-Yu Yang: 0000-0003-3454-3604

Author Contributions

W.G. carried out all the experiments. X.Y.Y. conceived the project, provided the idea, and designed and guided the experiments. B.L.S. conceived the project and supported scientific and technological platforms. N.J. taught the knowledge of cell culture. G.Y.Q. and T.L.S. provided the technique and guidance of click chemistry. G.T. performed the TEM measurements. X.L.L. and L.Y.W. tested and analyzed all the NMR spectra. Y.M. simulated the heat diffusion. W.G. and X.Y.Y. wrote and revised the paper. L.W., C.J., and G.Z. revised the paper. H.J.B. organized, wrote, and revised the paper. All the authors discussed results and analyzed the data.

Notes

The authors declare no competing financial interest.

ACKNOWLEDGMENTS

This work was supported by NSFC (51861135313, U1663225, U1662134, 21711530705, 21673282, 21473246), FRFCU (19lgpy112, 19lgzd16), National Key R&D Program of China (2017YFC1103800), PCSIRT (IRT_15R52), ISTCP (2015DFE52870), and JPSTDP (20180101208JC). We thank Prof. Fan Xia for QCM support at China University of Geosciences (Wuhan). H.J.B. is also director of the consulting company SASA BV.

DOI: 10.1021/acsnano.9b08108
ACS Nano 2019, 13, 14459−14467

REFERENCES

(1) Gawad, C.; Koh, W.; Quake, S. R. Single-Cell Genome Sequencing: Current State of the Science. *Nat. Rev. Genet.* **2016**, *17*, 175−188.

(2) Dubilier, N.; McFall-Ngai, M.; Zhao, L. Create a Global Microbiome Effort. *Nature* **2015**, *526*, 631−634.

(3) Fakhrullin, R. F.; Choi, I. S.; Lvov, Y. *Cell Surface Engineering: Fabrication of Functional Nanoshells*; Royal Society of Chemistry: Cambridge, 2014.

(4) Drachuk, I.; Gupta, M. K.; Tsukruk, V. V. Biomimetic Coatings to Control Cellular Function through Cell Surface Engineering. *Adv. Funct. Mater.* **2013**, *23*, 4437−4453.

(5) Liu, Z.; Xu, X.; Tang, R. Improvement of Biological Organisms Using Functional Material Shells. *Adv. Funct. Mater.* **2016**, *26*, 1862−1880.

(6) Park, J. H.; Hong, D.; Lee, J.; Choi, I. S. Cell-in-Shell Hybrids: Chemical Nanoencapsulation of Individual Cells. *Acc. Chem. Res.* **2016**, *49*, 792−800.

(7) Fakhrullin, R. F.; Zamaleeva, A. I.; Minullina, R. T.; Konnova, S. A.; Paunov, V. N. Cyborg Cells: Functionalisation of Living Cells with Polymers and Nanomaterials. *Chem. Soc. Rev.* **2012**, *41*, 4189−4206.

(8) Geng, W.; Wang, L.; Jiang, N.; Cao, J.; Xiao, Y.-X.; Wei, H.; Yetisen, A. K.; Yang, X.-Y.; Su, B.-L. Single Cells in Nanoshells for the Functionalization of Living Cells. *Nanoscale* **2018**, *10*, 3112−3129.

(9) Kim, B. J.; Cho, H.; Park, J. H.; Mano, J. F.; Choi, I. S. Strategic Advances in Formation of Cell-in-Shell Structures: From Syntheses to Applications. *Adv. Mater.* **2018**, *30*, 1706063.

(10) Jiang, N.; Yang, X.-Y.; Ying, G.-L.; Shen, L.; Liu, J.; Geng, W.; Dai, L.-J.; Liu, S.-Y.; Cao, J.; Tian, G.; Sun, T.-L.; Li, S.-P.; Su, B.-L. "Self-Repairing" Nanoshell for Cell Protection. *Chem. Sci.* **2015**, *6*, 486−491.

(11) Song, R.-B.; Wu, Y.; Lin, Z.-Q.; Xie, J.; Tan, C. H.; Loo, J. S. C.; Cao, B.; Zhang, J.-R.; Zhu, J.-J.; Zhang, Q. Living and Conducting: Coating Individual Bacterial Cells with *In Situ* Formed Polypyrrole. *Angew. Chem., Int. Ed.* **2017**, *56*, 10516−10520.

(12) Sakimoto, K. K.; Wong, A. B.; Yang, P. Self-Photosensitization of Nonphotosynthetic Bacteria for Solar-to-Chemical Production. *Science* **2016**, *351*, 74−77.

(13) Ji, Z.; Zhang, H.; Liu, H.; Yaghi, O. M.; Yang, P. Cytoprotective Metal-Organic Frameworks for Anaerobic Bacteria. *Proc. Natl. Acad. Sci. U. S. A.* **2018**, *115*, 10582−10587.

(14) Zhang, H.; Liu, H.; Tian, Z.; Lu, D.; Yu, Y.; Cestellos-Blanco, S.; Sakimoto, K. K.; Yang, P. Bacteria Photosensitized by Intracellular Gold Nanoclusters for Solar Fuel Production. *Nat. Nanotechnol.* **2018**, *13*, 900−905.

(15) Kim, H.; Shin, K.; Park, O. K.; Choi, D.; Kim, H. D.; Baik, S.; Lee, S. H.; Kwon, S.-H.; Yarema, K. J.; Hong, J.; Hyeon, T.; Hwang, N. S. General and Facile Coating of Single Cells *via* Mild Reduction. *J. Am. Chem. Soc.* **2018**, *140*, 1199−1202.

(16) Youn, W.; Ko, E. H.; Kim, M.-H.; Park, M.; Hong, D.; Seisenbaeva, G. A.; Kessler, V. G.; Choi, I. S. Cytoprotective Encapsulation of Individual Jurkat T Cells within Durable TiO_2 Shells for T-Cell Therapy. *Angew. Chem., Int. Ed.* **2017**, *56*, 10702−10706.

(17) Wang, L.; Hu, Z.-Y.; Yang, X.-Y.; Zhang, B.-B.; Geng, W.; Van Tendeloo, G.; Su, B.-L. Polydopamine Nanocoated Whole-Cell Asymmetric Biocatalysts. *Chem. Commun.* **2017**, *53*, 6617−6620.

(18) Jiang, N.; Yang, X.-Y.; Deng, Z.; Wang, L.; Hu, Z.-Y.; Tian, G.; Ying, G.-L.; Shen, L.; Zhang, M.-X.; Su, B.-L. A Stable, Reusable, and Highly Active Photosynthetic Bioreactor by Bio-Interfacing an Individual Cyanobacterium with a Mesoporous Bilayer Nanoshell. *Small* **2015**, *11*, 2003−2010.

(19) Kim, J. Y.; Lee, B. S.; Choi, J.; Kim, B. J.; Choi, J. Y.; Kang, S. M.; Yang, S. H.; Choi, I. S. Cytocompatible Polymer Grafting from Individual Living Cells by Atom-Transfer Radical Polymerization. *Angew. Chem., Int. Ed.* **2016**, *55*, 15306−15309.

(20) Niu, J.; Lunn, D. J.; Pusuluri, A.; Yoo, J. I.; O'Malley, M. A.; Mitragotri, S.; Soh, H. T.; Hawker, C. J. Engineering Live Cell Surfaces with Functional Polymers *via* Cytocompatible Controlled Radical Polymerization. *Nat. Chem.* **2017**, *9*, 537−545.

(21) Mao, A. S.; Shin, J.-W.; Utech, S.; Wang, H.; Uzun, O.; Li, W.; Cooper, M.; Hu, Y.; Zhang, L.; Weitz, D. A. Deterministic Encapsulation of Single Cells in Thin Tunable Microgels for Niche Modelling and Therapeutic Delivery. *Nat. Mater.* **2017**, *16*, 236−243.

(22) Leroux, G.; Neumann, M.; Meunier, C. F.; Fattaccioli, A.; Michiels, C.; Arnould, T.; Wang, L.; Su, B.-L. Hybrid Alginate@TiO_2 Porous Microcapsules as a Reservoir of Animal Cells for Cell Therapy. *ACS Appl. Mater. Interfaces* **2018**, *10*, 37865−37877.

(23) Zhou, H.; Wang, G.; Wang, X.; Song, Z.; Tang, R. Mineralized State of the Avian Influenza Virus in the Environment. *Angew. Chem., Int. Ed.* **2017**, *56*, 12908−12912.

(24) Guo, J.; Suástegui, M.; Sakimoto, K. K.; Moody, V. M.; Xiao, G.; Nocera, D. G.; Joshi, N. S. Light-Driven Fine Chemical Production in Yeast Biohybrids. *Science* **2018**, *362*, 813−816.

(25) Liang, K.; Richardson, J. J.; Cui, J.; Caruso, F.; Doonan, C. J.; Falcaro, P. Metal-Organic Framework Coatings as Cytoprotective Exoskeletons for Living Cells. *Adv. Mater.* **2016**, *28*, 7910−7914.

(26) Liang, K.; Richardson, J. J.; Doonan, C. J.; Mulet, X.; Ju, Y.; Cui, J.; Caruso, F.; Falcaro, P. An Enzyme-Coated Metal-Organic Framework Shell for Synthetically Adaptive Cell Survival. *Angew. Chem., Int. Ed.* **2017**, *56*, 8510−8515.

(27) Li, W.; Liu, Z.; Liu, C.; Guan, Y.; Ren, J.; Qu, X. Manganese Dioxide Nanozymes as Responsive Cytoprotective Shells for Individual Living Cell Encapsulation. *Angew. Chem., Int. Ed.* **2017**, *56*, 13661−13665.

(28) Park, J. H.; Kim, K.; Lee, J.; Choi, J. Y.; Hong, D.; Yang, S. H.; Caruso, F.; Lee, Y.; Choi, I. S. A Cytoprotective and Degradable Metal-Polyphenol Nanoshell for Single-Cell Encapsulation. *Angew. Chem., Int. Ed.* **2014**, *53*, 12420−12425.

(29) Li, W.; Bing, W.; Huang, S.; Ren, J.; Qu, X. Mussel Byssus-Like Reversible Metal-Chelated Supramolecular Complex Used for Dynamic Cellular Surface Engineering and Imaging. *Adv. Funct. Mater.* **2015**, *25*, 3775−3784.

(30) Kollár, R.; Reinhold, B. B.; Petráková, E.; Yeh, H. J. C.; Ashwell, G.; Drgonová, J.; Kapteyn, J. C.; Klis, F. M.; Cabib, E. Architecture of the Yeast Cell Wall: β (1→ 6)-Glucan Interconnects Mannoprotein, β (1→ 3)-Glucan, and Chitin. *J. Biol. Chem.* **1997**, *272*, 17762−17775.

(31) Bull, S. D.; Davidson, M. G.; van den Elsen, J. M. H.; Fossey, J. S.; Jenkins, A. T. A.; Jiang, Y.-B.; Kubo, Y.; Marken, F.; Sakurai, K.; Zhao, J.; James, T. D. Exploiting the Reversible Covalent Bonding of Boronic Acids: Recognition, Sensing, and Assembly. *Acc. Chem. Res.* **2013**, *46*, 312−326.

(32) Liu, H.; Li, Y.; Sun, K.; Fan, J.; Zhang, P.; Meng, J.; Wang, S.; Jiang, L. Dual-Responsive Surfaces Modified with Phenylboronic Acid-Containing Polymer Brush to Reversibly Capture and Release Cancer Cells. *J. Am. Chem. Soc.* **2013**, *135*, 7603−7609.

(33) Mori, H.; Miyamura, Y.; Endo, T. Synthesis and Characterization of Water-Soluble Silsesquioxane-Based Nanoparticles by Hydrolytic Condensation of Triethoxysilane Derived from 2-Hydroxyethyl Acrylate. *Langmuir* **2007**, *23*, 9014−9023.

(34) Meng, G.; Paulose, J.; Nelson, D. R.; Manoharan, V. N. Elastic Instability of a Crystal Growing on a Curved Surface. *Science* **2014**, *343*, 634−637.

(35) Yang, X. Y.; Li, Z. Q.; Liu, B.; Klein-Hofmann, A.; Tian, G.; Feng, Y. F.; Ding, Y.; Su, D. S.; Xiao, F. S. Fish-in-Net" Encapsulation of Enzymes in Macroporous Cages for Stable, Reusable, and Active Heterogeneous Biocatalysts. *Adv. Mater.* **2006**, *18*, 410−414.

(36) Wu, W.; Giese, R. F.; van Oss, C. J. Stability *versus* Flocculation of Particle Suspensions in Water-Correlation with the Extended DLVO Approach for Aqueous Systems, Compared with Classical DLVO Theory. *Colloids Surf., B* **1999**, *14*, 47−55.

(37) Berry, V.; Saraf, R. F. Self-Assembly of Nanoparticles on Live Bacterium: An Avenue to Fabricate Electronic Devices. *Angew. Chem., Int. Ed.* **2005**, *44*, 6668−6673.

(38) Asri, L. A. T. W.; Crismaru, M.; Roest, S.; Chen, Y.; Ivashenko, O.; Rudolf, P.; Tiller, J. C.; van der Mei, H. C.; Loontjens, T. J. A.; Busscher, H. J. A Shape-Adaptive, Antibacterial-Coating of Immobilized Quaternary-Ammonium Compounds Tethered on Hyper-

DOI: 10.1021/acsnano.9b08108
ACS Nano 2019, 13, 14459−14467

branched Polyurea and its Mechanism of Action. *Adv. Funct. Mater.* **2014**, *24*, 346−355.
(39) Qiao, Z.-A.; Zhang, L.; Guo, M.; Liu, Y.; Huo, Q. Synthesis of Mesoporous Silica Nanoparticles *via* Controlled Hydrolysis and Condensation of Silicon Alkoxide. *Chem. Mater.* **2009**, *21*, 3823−3829.
(40) Jeong, U.; Wang, Y.; Ibisate, M.; Xia, Y. Some New Developments in the Synthesis, Functionalization, and Utilization of Monodisperse Colloidal Spheres. *Adv. Funct. Mater.* **2005**, *15*, 1907−1921.
(41) Diaspro, A.; Silvano, D.; Krol, S.; Cavalleri, O.; Gliozzi, A. Single Living Cell Encapsulation in Nano-Organized Polyelectrolyte Shells. *Langmuir* **2002**, *18*, 5047−5050.
(42) Qing, G.; Zhao, S.; Xiong, Y.; Lv, Z.; Jiang, F.; Liu, Y.; Chen, H.; Zhang, M.; Sun, T. Chiral Effect at Protein/Graphene Interface: A Bioinspired Perspective to Understand Amyloid Formation. *J. Am. Chem. Soc.* **2014**, *136*, 10736−10742.
(43) Duan, H.; Nie, S. Cell-Penetrating Quantum Dots Based on Multivalent and Endosome-Disrupting Surface Coatings. *J. Am. Chem. Soc.* **2007**, *129*, 3333−3338.
(44) Shi, Y.; Wan, Y.; Liu, R.; Tu, B.; Zhao, D. Synthesis of Highly Ordered Mesoporous Crystalline WS_2 and MoS_2 *via* a High-Temperature Reductive Sulfuration Route. *J. Am. Chem. Soc.* **2007**, *129*, 9522−9531.
(45) Hong, D.; Lee, H.; Ko, E. H.; Lee, J.; Cho, H.; Park, M.; Yang, S. H.; Choi, I. S. Organic/Inorganic Double-Layered Shells for Multiple Cytoprotection of Individual Living Cells. *Chem. Sci.* **2015**, *6*, 203−208.
(46) Matsusaki, M.; Kadowaki, K.; Nakahara, Y.; Akashi, M. Fabrication of Cellular Multilayers with Nanometer-Sized Extracellular Matrix Films. *Angew. Chem., Int. Ed.* **2007**, *46*, 4689−4692.

DOI: 10.1021/acsnano.9b08108
ACS Nano 2019, 13, 14459−14467